International Astronomy and Astrophysics Research Journal

Volume 4, Issue 4, Page 28-48, 2022; Article no.IAARJ.97349

On the Interaction of Buoyant Magnetic Structures with Convective Plumes

Abrar A. Ali [a*] **and Lara J. Silvers** [b]

[a] *Department of Mathematics and Physics, the Australian University, P.O. Box 1411, Safat 13015, Kuwait.*

[b] *Department of Mathematics, City, University of London, Northampton Square, London, EC1V 0HB, UK.*

Authors' contributions

This work was carried out in collaboration between both authors. Both authors read and approved the final manuscript.

Article Information

Open Peer Review History:
This journal follows the Advanced Open Peer Review policy. Identity of the Reviewers, Editor(s) and additional Reviewers, peer review comments, different versions of the manuscript, comments of the editors, etc are available here: https://www.sdiarticle5.com/review-history/97349

Original Research Article

Received: 11/11/2022
Accepted: 29/12/2022
Published: 30/12/2022

ABSTRACT

Motivated by the tachocline region within the Sun, we investigate the interaction of buoyant structures with convection in a numerical set-up that resembles the base of the solar convection zone, where the fully compressible, non-linear magnetohydrodynamics equations are solved. Fully-developed convective flows are prescribed, with particular attention paid to identifying the features established in the earlier studies of [1] and [2] where parameterisation of the small-scale turbulent pumping is imposed using mean-field approximation. Analysis of several magnetoconvection regimes in quasi-two-dimensions reveals that the equipartition criterion between kinetic and magnetic energy does contribute globally to the flux emergence process as fluctuating motions in turbulent flows become more energetic. However, results were found to be less pronounced in the three-dimensional simulations due to the effectively reduced fluctuations.

Keywords: Convection; instabilities; MHD; Sun: interior; Sun: magnetic fields.

**Corresponding author: E-mail: a.abrar@au.edu.kw;*

1 INTRODUCTION

Until the late 1970s, solar physicists situated the mechanism maintaining solar dynamo entirely in the highly-turbulent convection zone, where magnetic fields undergo repeated stretching and folding due to the underlying turbulence [3, 4, 5]. It was then realised that magnetic fields could not fully be generated in the convection zone as the field can feedback on the flow in such a way as to disrupt the regeneration rate of the magnetic field, and so leading to spatial and temporal inconsistencies with the magnetic features observed on the solar surface (see [6, 7] and references therein). The idea of an interface-type dynamo, partially situated in the stable overshoot layer just below the convective zone was put forward by [8], where the existence of a toroidal field in the tachocline was assumed due to the presence of important physical processes that can influence the generation and sustenance of a large-scale field.

This solar interface dynamo model was built on the mechanisms of magnetic field transport within the solar interior. In the convection zone, transport of flux is enhanced, relative to the underlying sub-adiabatic layer, due to turbulent convective motions [9, 10]. Poloidal magnetic fields are primarily expelled to the tachocline as a result of turbulent diffusivity, while the shear-generated toroidal components are believed to reside within the low diffusion environment in the tachocline [11, 12].

The non-linear interactions between compressible turbulence and the underlying, large-scale toroidal component of the magnetic field serve to transport magnetic flux into the stellar atmosphere. Emergence of magnetic flux tubes is considered to be triggered by instabilities of the field in the non-turbulent tachocline [13]. Most notably, the process driven by magnetic buoyancy instability due to an unstable vertical gradient of the horizontally aligned magnetic field, embedded in a gravitationally stratified compressible atmosphere [3]. However, there remain some uncertainties on the exact physical mechanisms that allow fairly strong magnetic structures to traverse the turbulent convection zone.

Inspired by the mechanism of magnetic flux emergence that yields the observed solar features, [1] conducted a pilot study of the effects of turbulent flux pumping on the evolution of buoyancy structures, in a framework resembling the base of the convection zone, proposing a possible mechanism of suppressing the field before magnetic buoyancy instabilities play a significant role in the emergence of flux tubes. Results from their numerical calculations establish an equipartition relation between the Alfvén speed of the magnetic field and the pumping velocity under which the evolution of the large-scale field is determined – only structures where the magnetic field strength is comparable to equipartition strength can overcome the turbulent pumping and emerge.

Following this, given that convective patterns are highly time-dependent, [2] built on the model of [1] to account for temporal characteristics of the magnetic flux pumping and explore its effect on the formation and evolution of magnetic structures. The rate of emergence of magnetic structures, as well as their strengths, were found to be related to the temporal characteristics of the imposed pumping. The results reported by [1] and [2] were based on mean-field approximations where a net transport of mean magnetic field, that results from the non-isotropic parts of the mean electromotive force expansion, is adapted to simplify the effects of turbulent convection.

Parametrisation of the small-scale turbulent pumping does reveal interesting properties relating to the emergence of magnetic structures throughout the convection zone. However, simplifications of the pumping mechanism may not capture the various physical factors that contribute to the overall dynamics of the magnetic field. The research presented in this paper will focus on exploring the conclusions in the studies of [1] and [2] in a more realistic attempt of modelling magnetoconvection, by establishing a radial pumping that arises naturally from the turbulent convective flow.

Previous studies have looked at such magnetoconvection interactions but focused on the role of turbulent convection in transporting and storing the underlying magnetic field [10, 14, 15, 16]. The work present here will aim to investigate the rise of magnetic structures through the turbulent convection zone, mainly focusing on the effect of the equipartition criterion established in the earlier work of [1] and [2], in a framework of fully compressible convection such that the contribution of several competing physical factors incorporate to the net outcome.

Despite that convection in two dimensions represents simplifications of the real-world three-dimensional convective problems, it provides an understanding of how the physical properties imply to three dimensions. Furthermore, two-dimensional simulations are relatively inexpensive in terms of computational power than three-dimensional simulations. Thus, as a first step in understanding the problem, quasi-two-dimensional numerical experiments of compressible magnetohydrodynamics are performed. This is followed by numerical simulations extended to three dimensions, to explore and compare with the quasi two-dimensional findings.

This paper will proceed as follows: Section 2 outlines the model, parameter selection, and numerical approach. Section 3 discusses the results and this is followed by the conclusions in Section 4.

2 THE MODEL

A localised Cartesian system of a plane-parallel layer of compressible fluid is considered, where the dynamical evolution is described by the set of coupled, non-linear MHD equations in non-dimensional form. The layer extends from $0 \leq x \leq \lambda_x$ and $0 \leq y \leq \lambda_y$ in the horizontal directions, and $0 \leq z \leq d$ increases vertically downwards, parallel to the constant gravitational acceleration (refer to Fig. 1 for an illustration). Throughout the domain, the fluid is assumed to satisfy the perfect gas law with the dynamic viscosity, μ, the magnetic diffusivity, η, the gravitational force, g, the specific heats at constant density and pressure, c_v and c_p respectively, all constant. Thus, the set of non-dimensional compressible MHD equations reads

$$\frac{\partial \rho}{\partial t} + \nabla \cdot (\rho \mathbf{u}) = 0, \tag{2.1}$$

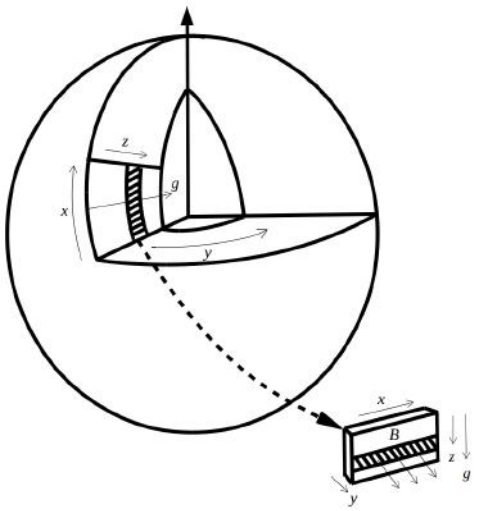

Fig. 1. A schematic representation of the Cartesian plane considered for the model

$$\rho\left(\frac{\partial \mathbf{u}}{\partial t} + (\mathbf{u}\cdot\nabla)\mathbf{u}\right) = -\nabla p - \nabla\left(\frac{F|\mathbf{B}|^2}{2}\right) + F(\mathbf{B}\cdot\nabla)\mathbf{B} + \sigma C_k(\nabla\cdot\tau) + \rho g\hat{\mathbf{z}}, \tag{2.2}$$

$$\frac{\rho}{(\gamma_s - 1)}\left(\frac{\partial T}{\partial t} + (\mathbf{u}\cdot\nabla)T\right) = -p\nabla\cdot\mathbf{u} + \frac{\gamma_s C_k}{(\gamma_s - 1)}\nabla\cdot\left(K\nabla T\right) + C_k\left(F\zeta_0|\nabla\times\mathbf{B}|^2 + \frac{\sigma\tau^2}{2}\right), \tag{2.3}$$

$$\frac{\partial \mathbf{B}}{\partial t} = \nabla\times(\mathbf{u}\times\mathbf{B} - C_k\zeta_0\nabla\times\mathbf{B}), \tag{2.4}$$

$$\nabla \cdot \mathbf{B} = 0, \tag{2.5}$$

where

$$p = \rho T, \tag{2.6}$$

and

$$\tau_{ij} = \frac{\partial u_i}{\partial x_j} + \frac{\partial u_j}{\partial x_i} - \frac{2}{3}\frac{\partial u_k}{\partial x_k}\delta_{ij}. \tag{2.7}$$

In the above equations, ρ is the fluid density, p is the pressure, T is the temperature, $\mathbf{B}$ is the magnetic field and $\mathbf{u}$ is the fluid velocity. In keeping with the mathematical formalism of prior related studies (for example, [1, 2, 17]), the unit of length is scaled by the depth of the layer d. Density and temperature are scaled by their initial value at the upper surface, ρ_0 and T_0, respectively. Magnetic field is scaled by the magnitude of the initial magnetic field B_0. Velocities are scaled by the sound travel-time across the layer in terms of the isothermal sound speed, $\sqrt{(c_p - c_v)T_0}$, and is related to the unit of time $d/\sqrt{(c_p - c_v)T_0}$.

Initially, quasi-two-dimensional simulations will be performed, also known as 2.5D, by assuming no gradients of quantities in the y-direction, i.e. motion only exists in the $x - z$ plane. This will be followed by considering the full three-dimensional problem. In this specific model, the thermal conductivity, K, is assumed to be a function of depth and is scaled by its initial value at the upper surface, K_0. Following this, several non-dimensional control parameters are obtained. These include the Prandtl number $\sigma = \mu c_p/K_0$, the dimensionless thermal diffusivity $C_k = K_0/\rho_0 c_p d\sqrt{(c_p - c_v)T_0}$, the ratio of magnetic to thermal diffusivity at the top of the layer $\zeta_0 = \eta c_p \rho_0/K_0$, the ratio of specific heats $\gamma_s = c_p/c_v$, and lastly the dimensionless field strength $F = {B_0}^2/(c_p - c_v)T_0\rho_0\mu_0$.

The computational domain is split into two piecewise polytropic layers to achieve a penetrative convection configuration, and mimic the interface region between the radiative zone and the convection zone. This is such that the top layer $0 \leq z \leq d/2$ is convectively unstable, and the bottom layer $d/2 \leq z \leq d$ is stable, with a smooth transition between the unstable layer and the stable layer, achieved by a hyperbolic tangent profile. This is obtained as in earlier works (see [16, 18, 19]) via a depth-dependent thermal conductivity as

$$K(z) = \frac{1}{2}\left[\left(\frac{m_B + 1}{m_T + 1} + 1\right) + \left(\frac{m_B + 1}{m_T + 1} - 1\right)\tanh\left(\frac{z - (d/2)}{0.1}\right)\right], \tag{2.8}$$

where m_T and m_B denote the polytropic indices of the top and bottom layers respectively. This approach was adapted in several previous investigations to account the effect of overshooting motions via penetrative convection on the stably stratified region below the convection zone.

For convective instability, the super-adiabatically stratified medium must satisfy $m < 3/2$ for a monoatomic perfect gas [20]. With the effect of adiabatic expansion (compression) of an ideal gas taken into account, the form of the dimensionless Rayleigh number, Ra, that determines the onset of buoyancy-driven convection in this framework is explicitly given by

$$Ra = \frac{(m_T + 1)\theta^2}{\sigma C_k^2 \gamma}(m_T + 1 - \gamma m_T)(1 + (\theta d)/4)^{(2m_T - 1)}, \tag{2.9}$$

where the Ra values quoted in this work are evaluated at the middle of the upper convective layer.

The system is assumed to satisfy periodic boundary conditions in the horizontal directions. The conditions at the upper and lower boundaries are such that the system is impermeable, stress-free and the magnetic field is vertical. Temperature is fixed at the upper surface, whilst heat flux is assumed to be a constant at the lower surface. Thus the boundary conditions in this framework are

$$\begin{aligned} u_z = \frac{\partial u_x}{\partial z} = \frac{\partial u_y}{\partial z} = B_x = B_y = 0, \quad T = T_0 \text{ at } z = 0, \\ u_z = \frac{\partial u_x}{\partial z} = \frac{\partial u_y}{\partial z} = B_x = B_y = 0, \quad \frac{\partial T}{\partial z} = \frac{m_T + 1}{m_B + 1}\frac{\theta T_0}{d} \text{ at } z = d, \end{aligned} \tag{2.10}$$

where the constant heat flux at the bottom of the domain is modified to account for the composite polytropic domain.

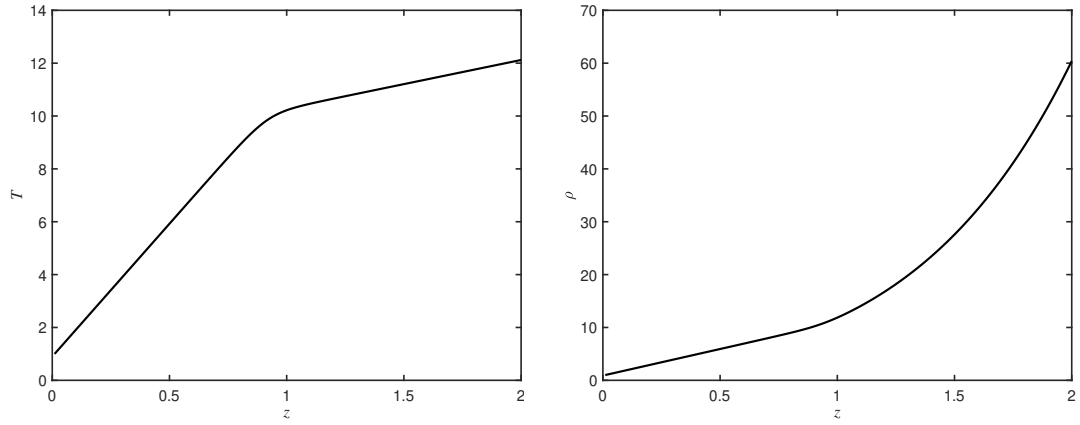

Fig. 2. Initial background states of temperature (left panel) and density (right panel) for $d = 2$, $T_0 = 1$, $\rho_0 = 1$, $\theta = 10$ with $m_T = 1$ and $m_B = 9$

For all calculations, an initial hydrostatic state is chosen by setting $\mathbf{u} = 0$. Accordingly, the equilibrium solutions for $\rho(z)$ and $T(z)$ are found numerically given the non-linearity of the static state thermal profile in this model. The equilibrium solution is shown in Fig. 2 for some value of m_T, m_B, θ, and d.

A uniform horizontal magnetic field $\mathbf{B} = B_y\hat{\mathbf{y}}$ is introduced into the existing hydrodynamic state, in the region bounded by $z = z_1$ and $z = z_2$, at later stages once convection has attained a statistically stationary state. To accommodate the imposed field, the density in the magnetic layer is adjusted so that the system is in equilibrium. This initial configuration is adapted together with the addition of small, random perturbations in the temperature profile. The equations are solved numerically using a parallel hybrid finite-difference/pseudo-spectral code. Time discretization is carried out based on an explicit, third-order Adams-Bashforth scheme, whilst spatial discretization is performed using fourth-order finite-differences in the vertical direction (upwind derivatives being used for the advection terms) and fast Fourier transforms in the horizontal directions. All simulations, described below, are carried out using a spatial resolution of $256 \times n_y \times 400$, where $n_y = 1$ for the quasi two-dimensional simulations and $n_y = 256$ for the three-dimensional simulations. More detail on the numerical set-up can be found in [21].

This model problem is governed by a number of non-dimensional quantities, which leads to a broad parametric space that requires large numerical efforts. In the solar context, the parameter settings are not known exactly, but rather a range of estimates for the parameters are available (see, for example, [12]). For instance, in the lower parts of the convection zone, the Prandtl number is of order 10^{-6} or less [22, 23]. Current numerical limitations do not allow to simulate the extreme values within the Sun; however the aim is to gain an insight into the underlying physics by choosing appropriate parameter values. The parameter choices are outlined in Table 1.

With the primary objective of simulating turbulent magnetoconvection, a supercritical convection is considered by setting the thermal stratification $\theta = 10$, specific gas $\gamma_s = 5/3$, thermal diffusivity $C_k = 0.07$, and Prandtl number $\sigma \leq 0.5$. A penetrative configuration is achieved, via the depth-dependent thermal conductivity profile in Eq. (2.8), by considering a convectively unstable top layer with polytropic index $m_T = 1$, and a convectively stable bottom layer with polytropic index $m_B = 9$. As described earlier, the horizontal magnetic layer will be introduced in the convectively stable region, with an initial magnetic field magnitude $B_y = 1$, magnetic diffusivity $\zeta_0 = 0.1$, and magnetic field strength F chosen to vary to explore its dependence on flux emergence.

Table 1. The choice of parameters for the magnetoconvection model

Parameter	Description	Value
σ	Prandtl number	Variable
C_k	Thermal diffusivity	0.07
θ	Thermal stratification	10.0
γ_s	Ratio of specific heats	5/3
ζ_0	Magnetic diffusivity	0.1
F	Magnetic field strength	Variable
m_T, m_B	Polytropic indicies	1.0, 9.0
z_1, z_2	Top and bottom of magnetic layer	1.35, 1.65
λ_x, λ_y	Box horizontal aspect ratio	6.0, 6.0
d	Vertical depth of box	2.0
B_y	Initial Horizontal magnetic strength	1.0

3 RESULTS

3.1 Quasi Two-Dimensional Simulations

The investigation is initiated by restricting attention to quasi two-dimensional simulations, where the hydrodynamic evolution of the system is focused upon to establish a convective motion before imposing a magnetic layer. The topological structure of the penetrative compressible convection can be seen in Fig. 3 for the parameter settings in Table 1 with $\sigma = 0.01$, which shows snapshots of the vertical velocity, w, and enstrophy density (vorticity squared), $\omega^2 = (\nabla \times \mathbf{u})^2$, at a single computational time.

For the w-velocity field, the colours red and blue denote upward and downward motions respectively. The enstrophy density highlights the intensity of the vorticity field, where bright and opaque colours denote strong values of the field, whereas weak values are more translucent. Most of the vorticity is generated at the interface between the stable and unstable regions. The motion in the upper convection layer is of asymmetric nature, with narrow regions of rapid downflow and broad regions of relatively slow upflow due to buoyancy braking. As reported by [24], such asymmetry is stemming from the combined effects of compressibility and stratification.

The background density stratification within the convectively unstable layer varies approximately by a factor of 5, and by a factor of 58 across the entire domain. The presence of the stably stratified lower layer decelerates the motion as it overshoots from above, in addition to reducing the strength of the overturning flow. It is to note that the convective plumes may continue to progress through the stable region, and are not confined to the upper part of the domain, and the extent of overshooting depends largely on the choice of parameters.

To relate the convection simulations to the γ-pumping in [1] and [2], we look at achieving a scale separation of the motion and extracting the fluctuation field. A simple way to obtain scale separation is by decomposing the velocity field in terms of mean and fluctuating parts [25, 26, 27]. Given that the pumping in the investigations of [1] and [2] was depth-dependent, we choose to look at the fluctuation field of the vertical velocity in the z-direction. Fig. 4 displays temporal line graphs of the average w-velocity, $\bar{w}$, and the small-scale fluctuations, w', over horizontal coordinates for the parameters in Table 1 with $\sigma = 0.01$, and two additional turbulent flows with $\sigma = 0.1$ and 0.5. This is such that $Ra = 4.9 \times 10^6$, 4.9×10^5 and 9.8×10^4 respectively.

As expected, Fig. 4 shows that at high supercritical Rayleigh numbers non-linear effects lead to the further development of turbulence [28, 29], and so introduces greater variability in the field. The γ-pumping extracted in the previous work of [1] and [2], does seem appropriate to portray this small-scale turbulence of the field in a simplified manner and isolate the action of turbulence on the large-scale magnetic field. Note that the vertical fluctuation scales are extremely small, as opposed to the γ-pumping amplitudes imposed in [1] and [2]. This is due to the computationally feasible choices of Ra in this model, which are small compared to that of the Sun, where $Ra \sim 10^{20}$ [30].

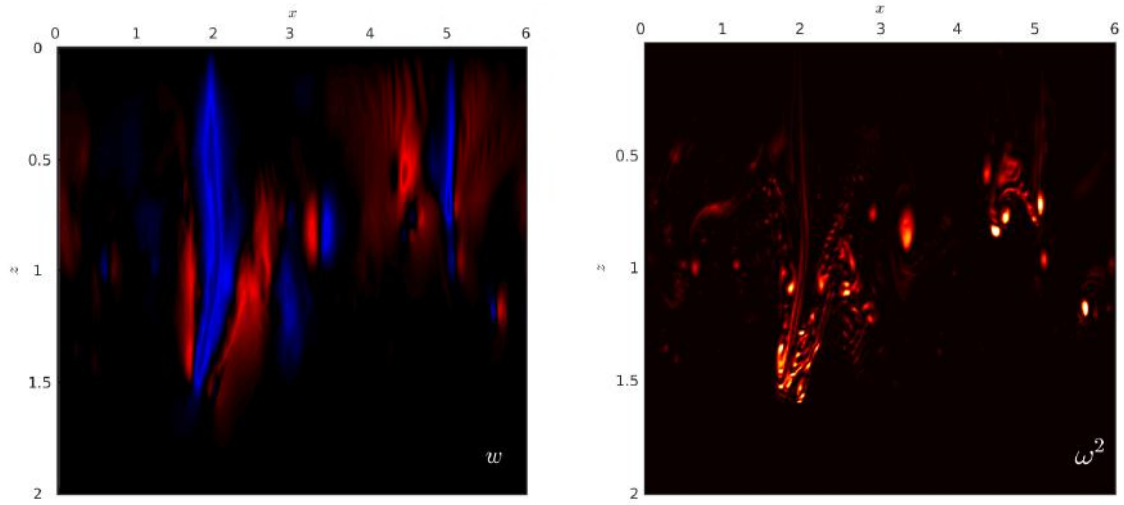

Fig. 3. Snapshots of the vertical velocity field (left panel) and enstrophy (right panel) for $\sigma = 0.01$ at a statistically steady state. The colours red and blue in the velocity field correspond to upward and downward convective motions respectively. Strong enstrophy densities are yellow, whereas weaker densities are dark and translucent

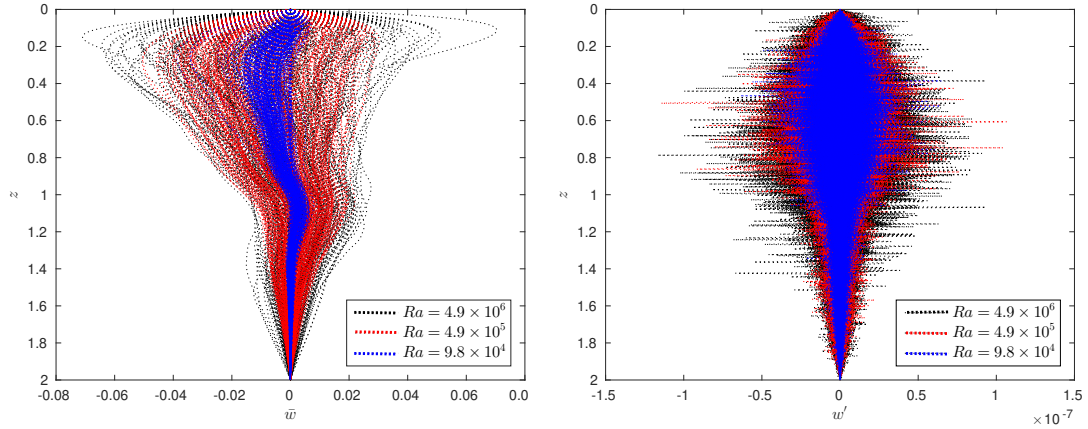

Fig. 4. Temporal line graphs of the average component (left panel) and fluctuating component (right panel) of the w-velocity field for several Ra values

As opposed to a dynamo-generated magnetic field (see, for example, [19, 31, 32]), the magnetic slab is introduced to the non-convective region, similar to the approach conducted by [10] and [16]. Once the convective flow has fully developed for $\sigma = 0.01$, the horizontally aligned magnetic field is inserted in the stable region of the domain. The magnetic field is imposed in the region $1.35 \leq z \leq 1.65$ by balancing the magnetic pressure and the gas pressure, to maintain the original pressure distribution. The discontinuity

in the initially imposed magnetic field rapidly leads to diffusion at the interface. More significantly, the field is susceptible to instabilities driven by magnetic buoyancy. The convective motion penetrating the stably stratified layer induces distortion in the magnetic layer, with some of the magnetic flux transported through the convection zone, while the bulk of the field is maintained in the overshoot region.

To highlight the magnetoconvection interactions, Fig. 5 shows snapshots of the horizontal component of the magnetic field, together with the vertical velocity field, for magnetic strength $F = 0.0001$. Initially, the field in Fig. 5(a) appears as a thin slab of strong horizontal magnetic field embedded in the lower region. After a short time, the buoyancy-driven magnetic field interacts with the overshooting convection. Magnetic flux can be seen to rise in Fig. 5(b), resulting from the combined effects of magnetic buoyancy and advection by the upflows (as indicated in red).

Fig. 5(c)-5(d) depict strong downward plumes piercing into the stable layer, with local magnetic field amplification occurring within the vicinity of the downflow due to stretching of the magnetic field lines, in addition to the complex interactions due to the small-scale vortical motions. This behaviour was also identified in [1] and [2] as the magnetic field interacts with the overlying downward turbulent pumping. The system acts to restrain the magnetic field in regions where the motion is downward. Fig. 5(f)-5(h) continue to show the dynamics of the magnetic field as it interacts with the overlying plumes, while for this very low value of F, the magnetic field is largely maintained in the stable layer.

To define the magnetic buckling effects as structures of sufficient strength that are able to overcome the convective region or simply the advection of the magnetic field by the flow in a passive manner, kinetic and magnetic energies need to become comparable (equipartition), given that the back reaction of the magnetic field becomes of significant importance [7, 33]. Magnetic fields need to achieve an equipartition strength with the flow, on a local scale, to escape through the convective motions, as found in the turbulent pumping model of [1] and [2], or otherwise are transported passively. Initially, on a global scale, the magnetic field appears to be a weak field. Though, this could give rise to local small-scale structure of the magnetic field with energy comparable to the kinetic energy of the flow.

To distinguish the behaviour of the magnetic field, the equipartition of energy is investigated by calculating the ratio of kinetic energy to magnetic energy in Fig. 6 for a case where the back reaction of the field onto the flow is $F = 0.1$. Values greater than unity suggest that the magnetic field is influenced by the surrounding convective motions, whereas values less than unity suggest that the magnetic field is able to resist the surrounding motions, and so rises. According to the equipartition measure, the magnetic field in Fig. 6(a) predominantly behaves with respect to the surrounding motions, which in this case causes buoyant magnetic structures to rise further. As time evolves, Fig. 6(b) reveals small-scale magnetic structures of equipartition strength developing at various regions in the domain. However, these structures do not progress further through the upper layer, as one would imagine, due to the frequent mixing of the overlying turbulent convection. The locality of the equipartition strength achieved by the magnetic field does not overcome the motion as the magnetic structure continues to rise.

From Fig. 6(c), less than 4% the strength of the initially imposed magnetic field emerged through the convective layer, as a result of magnetic buoyancy and advection by the upflows, with some stages where the magnetic energy overcomes the kinetic energy. Although earlier images reveal the intensification of the magnetic field in the lower part of the domain, the efficient rise of equipartition-strength magnetic structures as proposed in the investigations of [1] and [2] is not seen.

By increasing the strength of the field to $F = 1.0$, one allows magnetic structures of equipartition level to be reached easily. Fig. 7 reveals a stage where a magnetic structure escapes to the convective layer. From the equipartition plot, the magnetic energy overcomes the kinetic energy throughout the region of emergence, thus suggesting the rise of the magnetic field despite the surrounding convective motions. This behaviour continues at various locations in Fig. 7(a) and 7(b). However, these findings remain inadequate to conclude the emergence of magnetic structures, comparable to equipartition strength, throughout the convection zone. This is partially due to turbulent motions appearing weak when emergence takes place in the regime where the magnetic energy overcomes the kinetic energy – in addition to the possible contribution of increasing F, which involves amplitude reduction of convective motions in the traverse direction due to magnetic tension, and enhanced buoyancy effect of localised magnetic structures due to magnetic pressure [34].

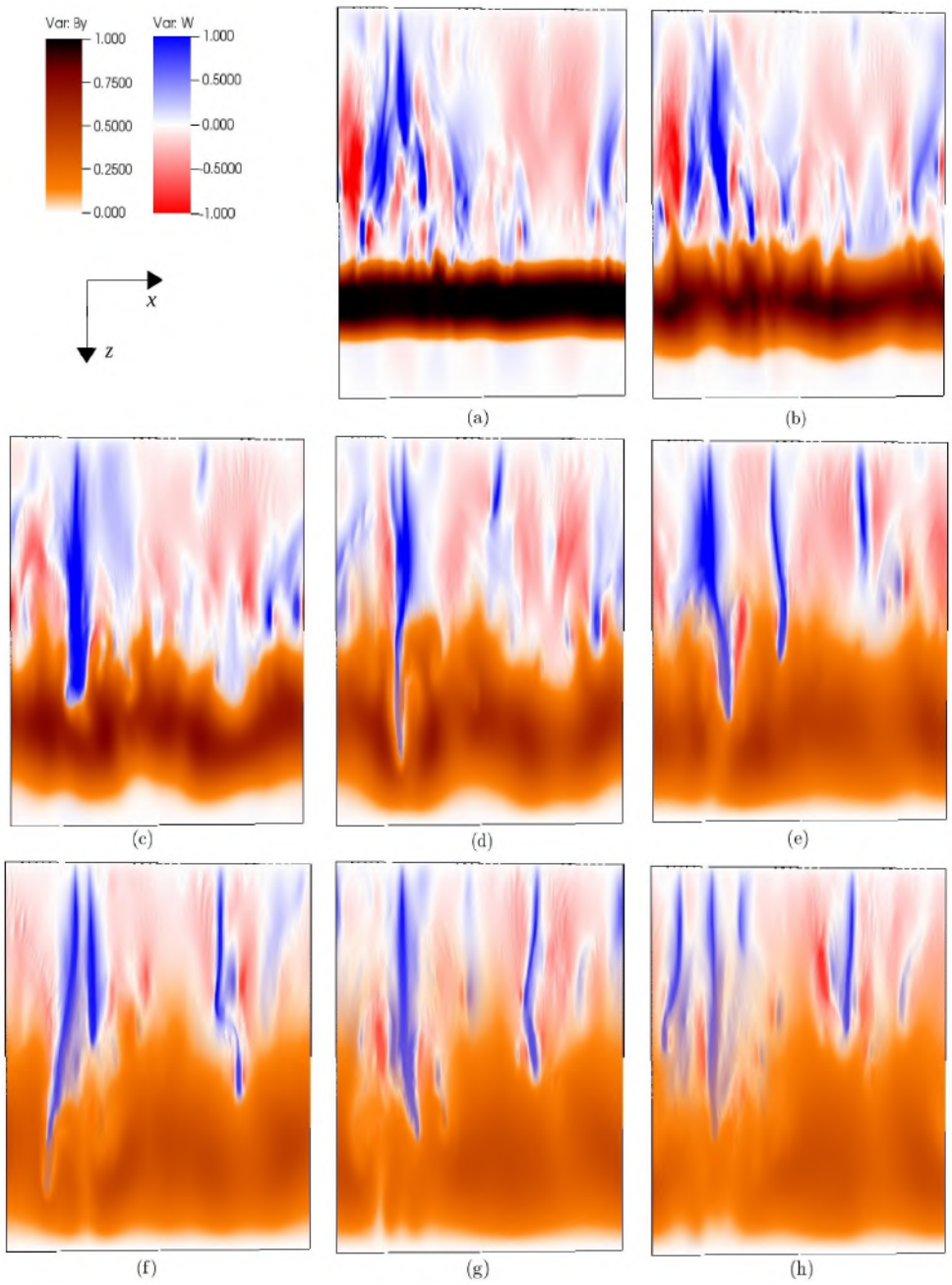

Fig. 5. Snapshots of the z-component of the velocity field overlaid with the y-component of the magnetic field at computational times (a) $t = 40.68$, (b) $t = 41.21$, (c) $t = 42.03$, (d) $t = 43.04$, (e) $t = 44.50$, (f) $t = 45.73$, (g) $t = 46.87$, and (h) $t = 47.92$ respectively.

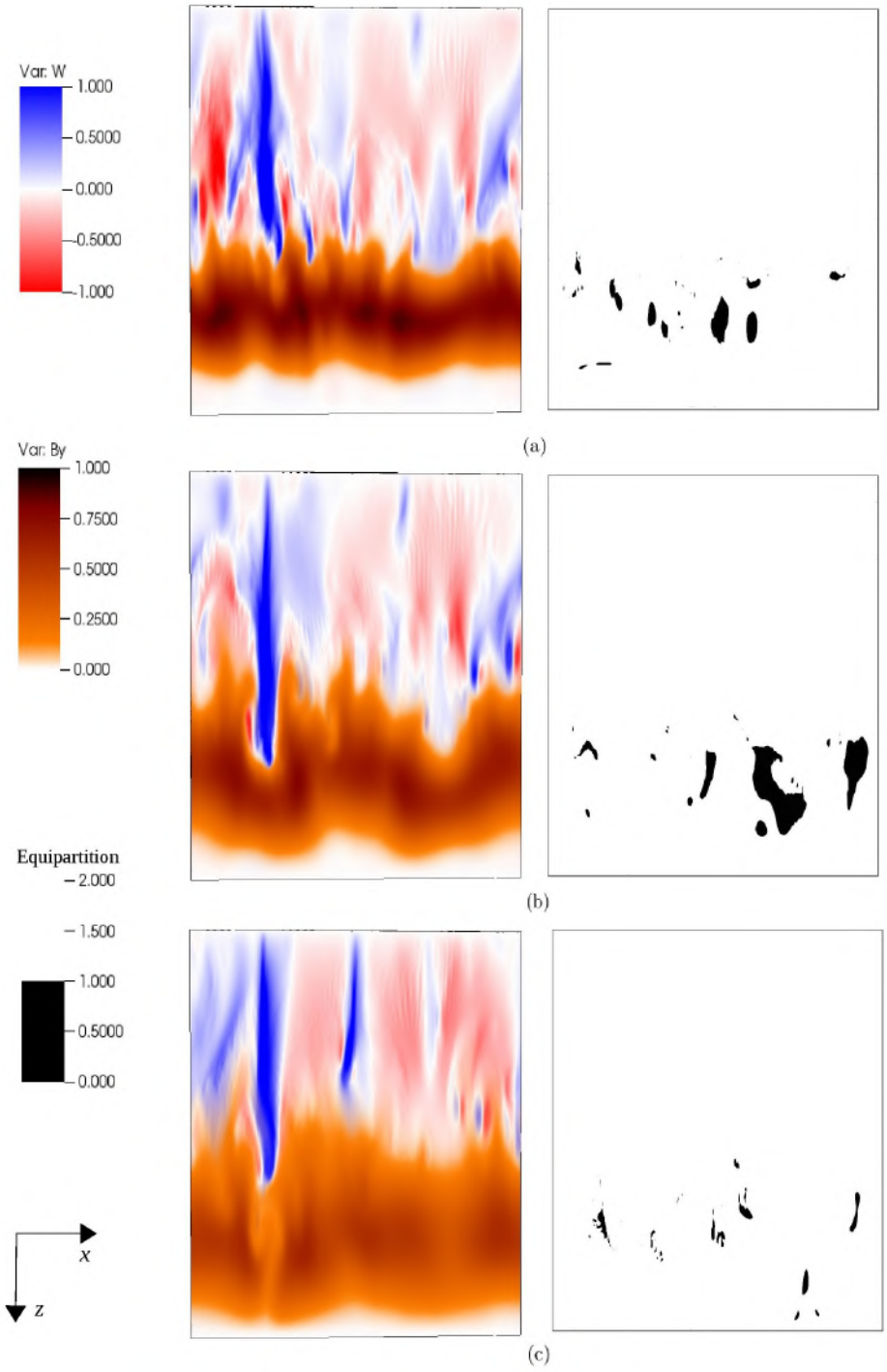

Fig. 6. Snapshots of the the z-component of the velocity field overlaid with the y-component of the magnetic field (left) and ratio of the kinetic to magnetic energy (right) at (a) $t = 40.68$, (b) $t = 41.21$, and (c) $t = 42.03$ respectively

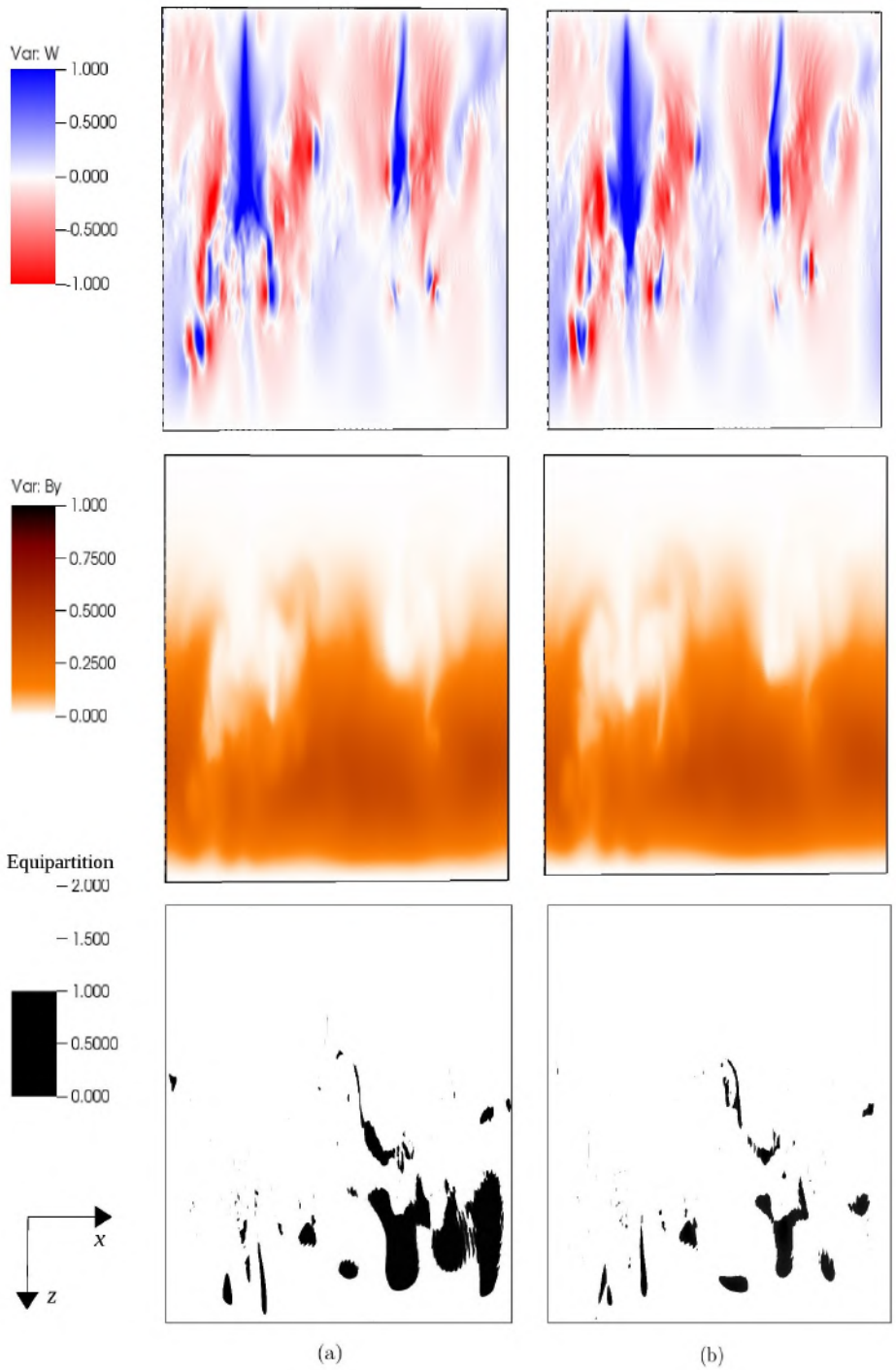

Fig. 7. Snapshots of the z-component of the velocity field (top), the y-component of the magnetic field (middle) and ratio of the kinetic to magnetic energy (bottom) at (a) $t = 46.31$ and (b) $t = 46.56$ respectively

The redistribution of the magnetic field is examined by calculating the evolution of the average horizontal magnetic field in the y-direction, for various magnetic strengths in the range $10^{-4} \leq F \leq 1$. Generally, the mean magnetic field plays a passive role for all cases and is relatively insensitive to the choices of F on a global scale, as was also identified in [10]. Fixing $F = 0.01$, we specifically discuss the analysis of the horizontally-averaged magnetic field for $\sigma = 0.01$ and $\sigma = 0.1$.

Fig. 8 shows the magnetic flux redistribution as line graphs for equally-spaced time intervals, and as colour-coded spacetime diagrams that display a colour, with respect to the amplitude of the magnetic field, in both space and time. For both flows, $\sigma = 0.01$ (top panel of Fig. 8) and $\sigma = 0.1$ (bottom panel of Fig. 8), the evolution starts with the magnetic field contained in the region where it is initially introduced (as displayed in solid line). The peak strength remains located within that region, while it decreases in magnitude as it spreads toward the unstable layer. Some of the flux can be seen to escape through the boundaries, hence reducing the total amount of magnetic flux. Additionally, as time evolves, the magnetic field decays in strength due to the absence of mechanisms that generate the field. This is expected as this model represents magnetoconvection rather than dynamo interactions.

From both line graphs and spacetime diagrams, greater dispersal of the magnetic field can be noticed for $\sigma = 0.01$. This is a result of the local amplification of the field in the more turbulent flow that leads to the emergence of small-scale, equipartition strength magnetic structures, in addition to the transport of the field by ascending flows.

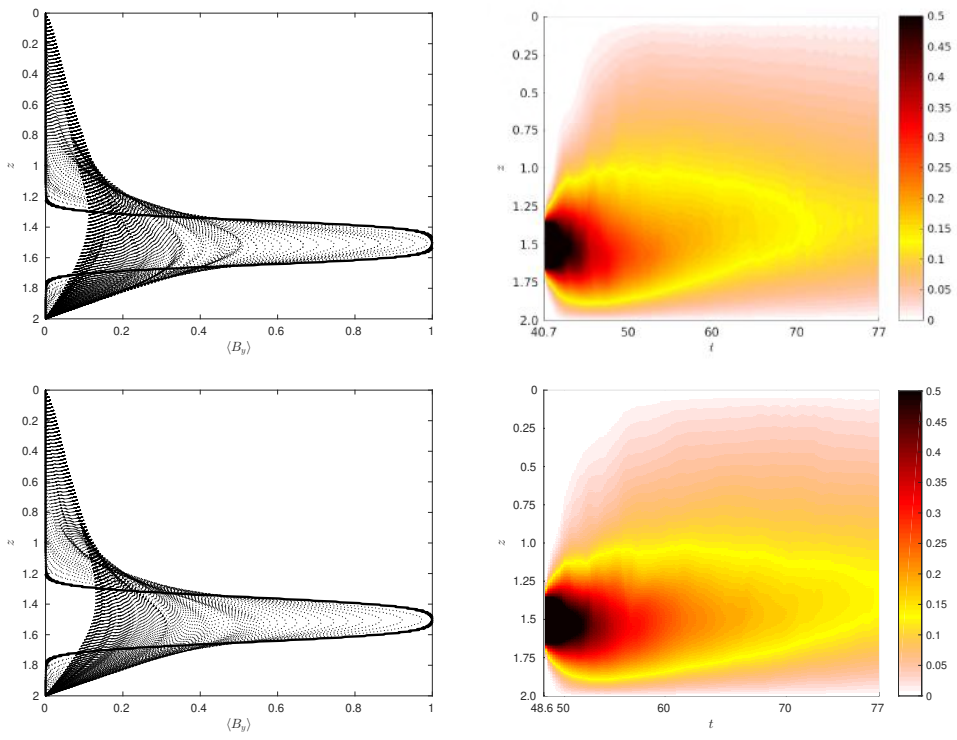

Fig. 8. Line graphs (left) and colour spacetime diagrams (right) of the horizontal average of the magnetic field in the y-direction, B_y for $\sigma = 0.01$ (top panel) and $\sigma = 0.1$ (bottom panel), where $F = 0.01$

The fraction of magnetic flux present in the part of the domain above the initial location of the magnetic field ($z_1 = 1.35$), and the measure of depth with respect to the maximum value are quantified by

$$\Phi = \int_0^{1.35} \langle B_y \rangle \, \mathrm{d}z \Big/ \int_0^{2} \langle B_y \rangle \, \mathrm{d}z \,, \tag{3.1}$$

and

$$z_{max} = z \Big| \max_z \langle B_y \rangle (z) \,, \tag{3.2}$$

respectively. Fig.9 displays Φ and z_{max}, for $\sigma = 0.01, 0.1$ and 0.5, for a fixed window of time after the field is imposed, in order to minimise the influence of the upper boundary as the simulation progresses. Given that the field is imposed at different computational times for each flow, time is normalised to unity to allow direct comparisons. Interestingly, as σ decreases (Ra increases), Φ reveals a greater proportion of magnetic flux in the upper layer during the early stages of the interaction. This indicates the contribution of the equipartition relation in transporting magnetic structures, which is more pronounced as the flow increases in turbulence (case $\sigma = 0.01$). However, as time evolves the strength of magnetic structures reduce, as noted in Fig. 8, and so equipartition-strength magnetic structures are unlikely to play a significant role. Therefore, these calculations suggest that advection becomes the predominant mechanism for magnetic field transport, where the least turbulent convective flow (case $\sigma = 0.5$) succeeds in carrying larger quantities of magnetic field throughout the upper domain.

The measure z_{max} emphasises the effectiveness of the overlying pumping on the imposed magnetic field. From all three cases of σ, strong concentrations of the field are shown to be maintained deeper, with respect to z, for flows where Ra is larger. This means that overshooting convective plumes are more efficient in pushing magnetic fields downwards in the case where $\sigma = 0.01$.

3.2 Three-Dimensional Simulations

To allow a fuller treatment of the problem, three-dimensional simulations are conducted for some of the cases considered in the preceding subsection. Several differences in the physical properties of the convective flow become apparent, as the 3D simulations are compared with their equivalent quasi 2D simulations. Snapshots of the vertical velocity for $\sigma = 0.1$ are shown in Fig. 10 in both quasi 2D and full 3D, at different stages in time once the convective patterns are developed. It emerges, from the vertical velocity field in quasi 2D and the horizontal cross-section at $y = 1$ in 3D, that plume structures become noticeably different near the interface region. In 3D, the flow is dominated by small convective structures, while contrastingly, quasi 2D reveals more coherency within the flow, in addition to the effective penetration towards the underlying stably stratified layer.

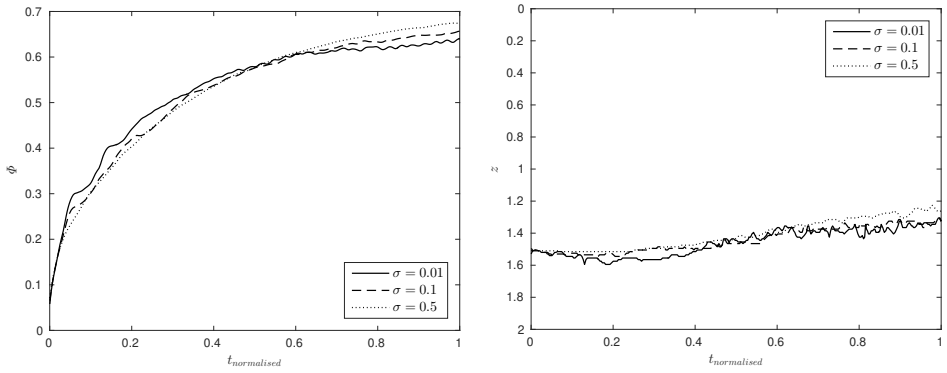

Fig. 9. The temporal evolution of the magnetic flux fraction contained above the initial location of magnetic field, Φ, (left panel) and the location of the maximum magnetic field, z_{max} (right panel)

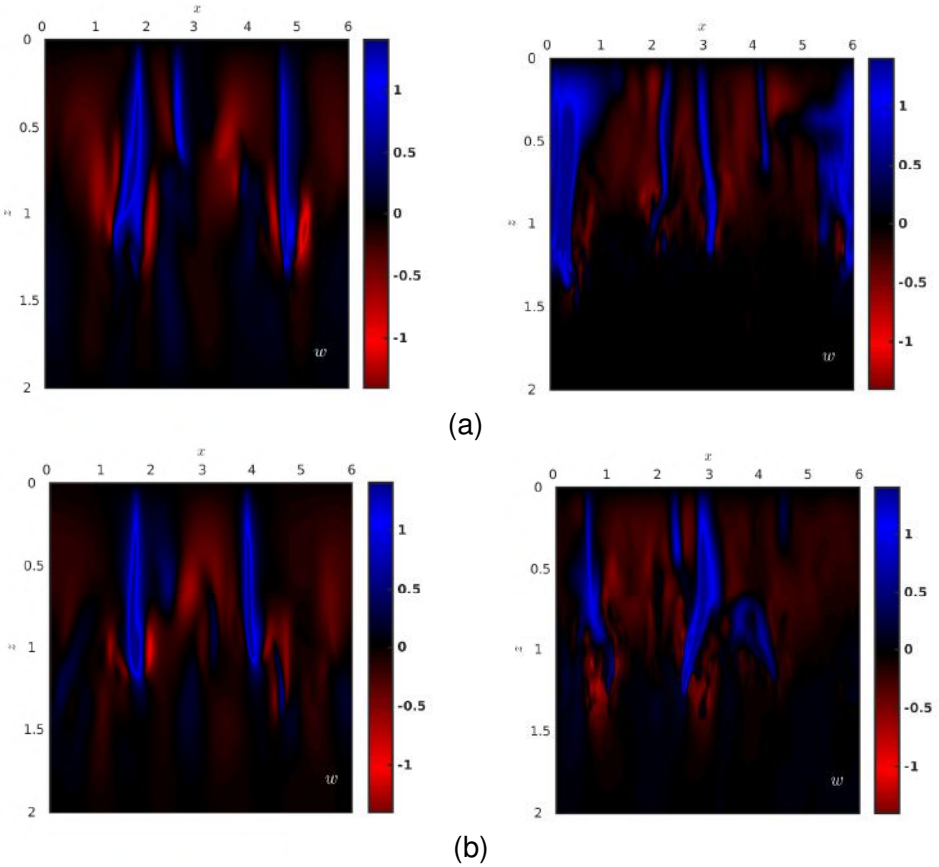

Fig. 10. The vertical velocity field at computational times (a) $t \approx 26$ and (b) $t \approx 35$ for the case $\sigma = 0.1$ in two dimensions (left) and three dimensions (right)

Evaluation of the horizontally average vertical velocity profiles in Fig. 11 depicts the substantial difference in transitioning from quasi 2D simulations to full 3D simulations. In the three-dimensional framework, the average vertical motion varies more smoothly in time, with smaller amplitudes in comparison to the more chaotic quasi 2D regime. The constrained motion in the two-dimensional plane triggers the accumulation of energy, as displayed in the kinetic energy profiles in Fig. 12, which consequently leads to the rapid variation of velocity in time. Analogous findings were also established in [35], where flows are consistently more turbulent in 2D, and converge at large Prandtl numbers.

To capture the dynamics associated with the transport of the magnetic field through the turbulent convecting region in three-dimensions, a horizontal magnetic layer is inserted at computational time $t \approx 42$, in the case where $\sigma = 0.1$ and $F = 0.01$. Snapshots of the 3D magnetoconvection interactions in Fig. 13 generally reveal similar characteristics to that determined in two-dimensions (Fig. 5). The effects of convection and turbulence can clearly be viewed in Fig. 13(a)-13(k), where the buoyancy-driven magnetic field undergoes suppression and amplification as it competes with the overlying convective motion to escape.

Fig. 14 highlights the equipartition-strength magnetic structures for the 3D simulation, by displaying snapshots of the vertical velocity, horizontal magnetic field, and ratio of kinetic energy to magnetic energy, at several computational times.

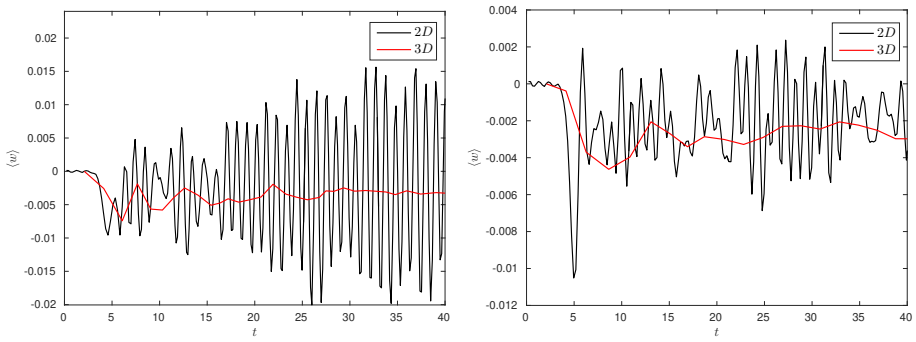

Fig. 11. Temporal evolution of the average vertical velocity for $\sigma = 0.1$ (left panel) and $\sigma = 0.5$ (right panel) in two and three dimensions

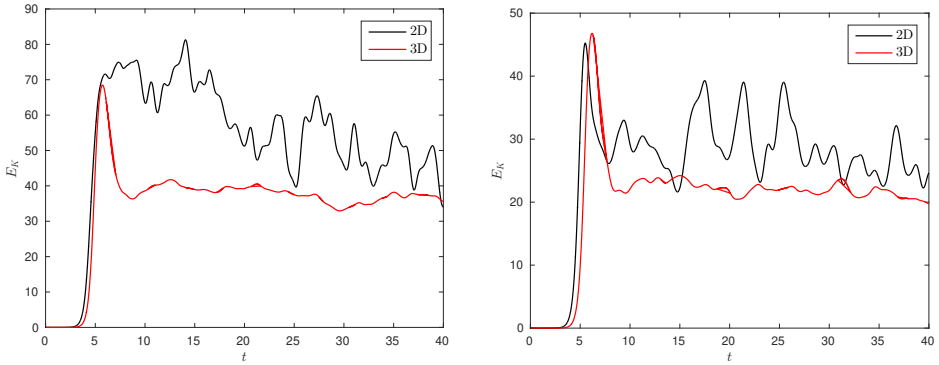

Fig. 12. Temporal evolution of the total kinetic energy for $\sigma = 0.1$ (left panel) and $\sigma = 0.5$ (right panel) in two and three dimensions

The transport of the magnetic field through the convective layer is predominantly a result of advection. Magnetic structures of equipartition-strength occur at the interface region, and almost remain within the lower domain as the strength of the field is insufficient to overcome the relatively stronger, overlying convective downflows. Therefore, to rise further through the domain, magnetic structures must be transported by the convective upflows.

Focusing on the global distribution of the magnetic field, Fig. 15 shows Φ and z_{max}, as defined in Equations (3.1) and (3.2) respectively, for $\sigma = 0.1$ and $\sigma = 0.5$. The magnetic field is found to behave differently, in comparison to the quasi 2D cases. Here, a smoother time evolution of the profiles Φ and z_{max} is noticed. This is expected, given the reduced turbulence as the additional dimension is introduced. For the least turbulent flow in 3D, $\sigma = 0.5$, a greater amount of magnetic field is present in the upper domain. This agrees with the pattern determined in the final stages of the quasi 2D evolution, where advection overtakes as the more active process in transporting the magnetic field, and so suggests that the degree of turbulence in the 3D cases is insufficient to highlight the contribution of equipartition-strength magnetic structures in enhancing the rate of flux emergence.

The profile of z_{max} reveals similar features to the earlier quasi 2D findings; maximum field strength is maintained deeper for turbulent flows of greater velocity fluctuations, in this case $\sigma = 0.1$.

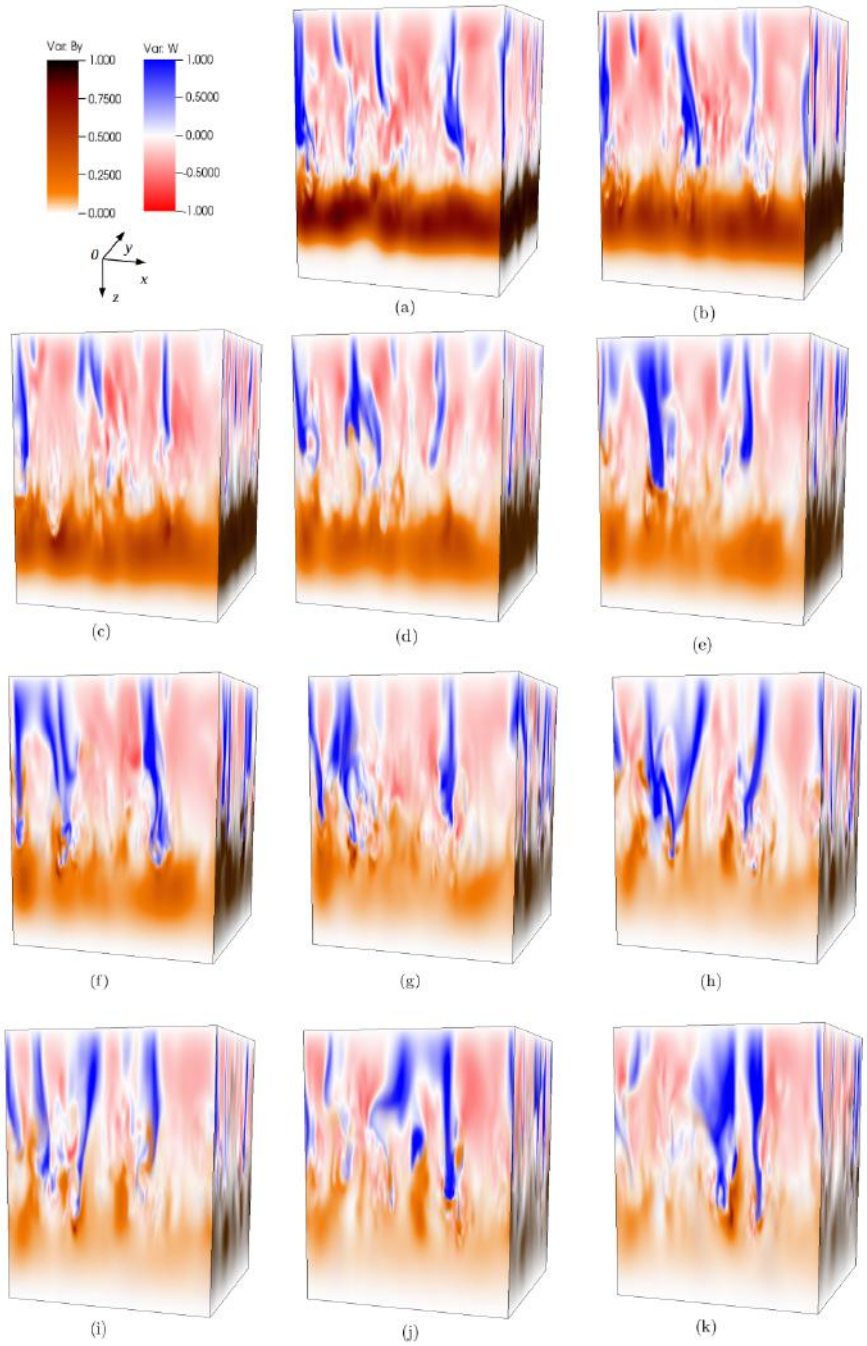

Fig. 13. Snapshots of the z-component of the velocity field overlaid with the y-component of the magnetic field in three dimensions at computational times (a) $t = 41.78$, (b) $t = 43.02$, (c) $t = 44.15$, (d) $t = 46.40$, (e) $t = 48.60$, (f) $t = 49.80$, (g) $t = 52.16$, (h) $t = 54.66$, (i) $t = 55.61$, (j) $t = 57.37$ and (k) $t = 58.69$ respectively

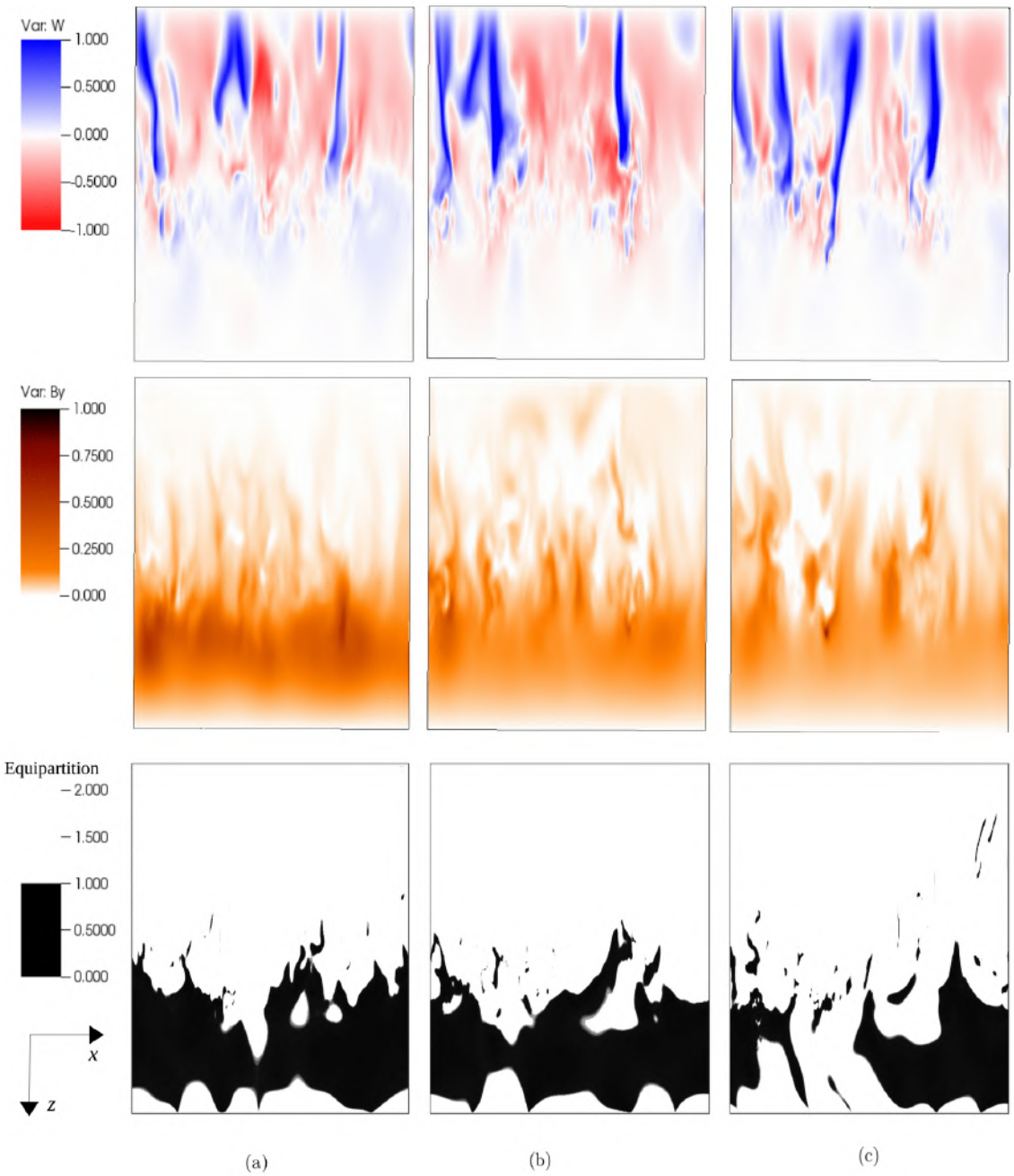

Fig. 14. Snapshots of the z-component of the velocity field (top), the y-component of the magnetic field (middle) and ratio of the kinetic to magnetic energy (bottom) at $y = 0$ for times (a) $t = 45.3$, (b) $t = 50.9$, and (c) $t = 55.6$ respectively

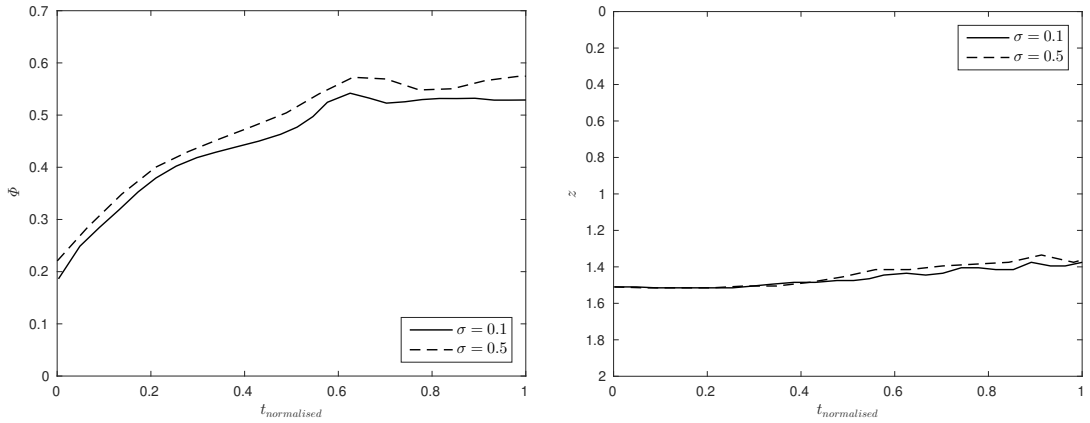

Fig. 15. The temporal evolution of the magnetic flux fraction contained above the initial location of magnetic field, Φ, (left panel) and the location of the maximum magnetic field, z_{max} (right panel)

4 CONCLUSIONS

Starting from the fundamentals of MHD and the key equations governing the interactions between electrically conducting fluid and magnetic field, an idealised numerical model is adapted to explore the non-linear interaction between convective flows and buoyancy-driven magnetic structures, in a regime resembling the solar interior where the convection zone meets the tachocline, and address the nature of rising magnetic structures that eventually form active regions when they reach the surface of the Sun. Initially, prior to exploring the MHD model, various convective flows were established with respect to the non-dimensional Rayleigh number. The magnetic field was later introduced in a stably stratified region, positioned below the convectively unstable region once the hydrodynamic convection was fully developed, and the evolution of the magnetic field was investigated.

The quasi-two-dimensional results revealed two possibilities to explain the behaviour of the rising magnetic field. It was found that the magnetic field, while it is largely maintained in the vicinity where it was initially prescribed, can rise passively via convective motions, or alternatively strong magnetic structures, comparable to the surrounding motions, can rise without getting distracted by the overlying complexities of convection as was shown in [1] and [2]. Given the extreme conditions in the solar interior, the second possibility is most likely to occur. However, this equipartition phenomenon was complicated and difficult to solidly highlight due to the limitation of the simplified model.

In the presented simulations, the transport of the field was mainly passive through the upper layer, but in the lower layer, it was observed that small-scale, equipartition strength magnetic structures were reached. These magnetic structures were easily captured for larger values of F and were found to escape fractionally, however, they cannot rise unhindered given the inescapable, larger velocities present further through the upper region. Hence, the only possible way to escape completely is through the combination of both mechanisms.

The equipartition criterion of [1] and [2] was found to appear on a local scale and does contribute towards the global behaviour of the magnetic field, particularly as the flow becomes more turbulent. Greater fluctuations in the velocity field revealed an increased fraction of magnetic flux escaping through the convection zone. This is a result of the effective pumping and local amplification of the field due to turbulence, which enhances the emergence of equipartition-strength magnetic structures. However, the absence of mechanisms for generating magnetic

fields led to a reduction in the magnetic field as time evolves. Consequently, the occurrence of equipartition-strength magnetic structures becomes less likely, and so advection overtakes as the primary source of field transport.

In this work, we also provided an insight into the magnetoconvection interactions in three dimensions by conducting some of the quasi-two-dimensional cases in three dimensions. The additional degree of freedom was found to smoothen the variability and reduce the fluctuations of the velocity field. Therefore, unlike the quasi-2D simulations, equipartition-strength magnetic structures were not found to globally contribute toward the transport of magnetic field through the overlying convective layer. Results in quasi-2D highlight the findings of [1] and [2], in terms of the effective role of turbulent pumping in transporting and maintaining the magnetic field. To capture similar dynamics to the quasi-2D calculations in 3D, further calculations of very high Rayleigh number turbulent convection must be investigated in 3D space, which numerically remains challenging.

It is important to note that due to the gap between numerical calculations and observations, our understanding of the Sun remains incomplete. The extreme conditions within the Sun cannot be retrieved in numerical simulations of convection, for instance. The desired Rayleigh number that portrays the property of convection in the solar interior cannot be simulated as the available computational capacity remains a major constraint to achieving the strong turbulence required. Therefore, the adaption of simplified models, such as the γ-pumping in [1] and [2], might be a better approach to shed further light on the effect of turbulence in the solar convection zone.

DISCLAIMER

This paper is an extended version of a repository document of the same author. The repository document is available in this link: https://openaccess.city.ac.uk/id/eprint/24159/1/ Ali%2C%20Abrar.pdf [As per journal policy repository article can be published as a journal article, provided it is not published in any other journal]

ACKNOWLEDGEMENT

This research has been financially supported by the Science and Technology Facilities Council (STFC) studentship award ST/M503459/1. The computations were performed using the solon supercomputer at City, University of London and the Cambridge Service for Data Driven Discovery (CSD3) part of which is operated by the University of Cambridge Research Computing on behalf of the STFC DiRAC HPC Facility (www.dirac.ac.uk). The DiRAC component of CSD3 was funded by BEIS capital funding via STFC capital grants ST/P002307/1 and ST/R002452/1 and STFC operations grant ST/R00689X/1. DiRAC is part of the National e-Infrastructure.

COMPETING INTERESTS

Authors have declared that no competing interests exist.

REFERENCES

[1] Barker AJ, Silvers LJ, Proctor MRE and Weiss NO. Magnetic buoyancy instabilities in the presence of magnetic flux pumping at the base of the solar convection zone. Mon. Not. Roy. Astron. Soc. 2012;424:115-127.

[2] Ali AA and Silvers LJ. The effect of time-dependent γ-pumping on buoyant magnetic structures. Geophys. Astrophys. Fluid Dyn. 2018;112:414-430.

[3] Parker EN. The formation of sunspot from the solar toroidal field. Astrophys. J. 1955a;121:491-507.

[4] Babcock HW. The topology of the Sun's magnetic field and the 22-year cycle. Astrophys. J. 1961;133:572-587.

[5] Steenbeck M and Krause F. On the dynamo theory of stellar and planetary magnetic fields. I. AC dynamos of solar type. Astron. Nachr. 1969;291:49-84.

[6] Parker EN. The generation of magnetic fields in astrophysical bodies. X - Magnetic buoyancy and the solar dynamo. Astrophys. J. 1975;198:205-210.

[7] Silvers LJ. Magnetic fields in astrophysical objects. Philos. T. Roy. Soc. 2008;366:4453-4464.

[8] Parker EN. A solar dynamo surface wave at the interface between convection and non-uniform rotation. Astrophys. J. 1993;408:707-719.

[9] MacGregor KB and Charbonneau P. Solar interface dynamos. I. Linear, kinematic models in

Cartesian geometry. Astrophys. J. 1997;486:484-501.

[10] Tobias SM, Brummell NH, Clune TL and Toomre J. Transport and storage of magnetic field by overshooting turbulent compressible convection. Astrophys. J. 2001;549:1183-1203.

[11] Hughes DW. Magnetic buoyancy instabilites in the tachocline. In: Hughes DW, Rosner R, Weiss NO, editors. The Solar Tachocline. 1st ed. Cambridge: Cambridge University Press; 2007.

[12] Priest E. Magnetohydrodynamics of the Sun. 1st ed. Cambridge: Cambridge University Press; 2014.

[13] Tobias SM and Weiss NO. The solar dynamo and the tachocline. In: Hughes DW, Rosner R, Weiss NO, editors. The Solar Tachocline. 1st ed. Cambridge: Cambridge University Press; 2007.

[14] Nordlund Å, Brandenburg A, Jennings RL, Rieutord M, Ruokolainen J and Stein RF. Dynamo action in stratified convection with overshoot. Astrophys. J. 1992;392:647-652.

[15] Brandenburg A, Jennings RL, Nordlund Å., Rieutord M, Stein RF and Tuominen I. Magnetic structures in a dynamo simulation. J. Fluid Mech. 1996;306:325-352.

[16] Tobias SM, Brummell NH, Clune TL and Toomre J. Pumping of magnetic fields by turbulent penetrative convection. Astrophys. J. 1998;502:L177-L180.

[17] Skinner DM and Silvers LJ. Double-diffusive magnetic buoyancy instability in a quasi-two-dimensional Cartesian geometry. Mon. Not. Roy. Astron. Soc. 2013;436:531-539.

[18] Hurlburt NE, Toomre J, Massaguer JM and Zahn J-P. Penetration below a convective zone. Astrophys. J. 1994;421:245-260.

[19] Silvers LJ, Bushby PJ, and Proctor MRE. Interactions between magnetohydrodynamic shear instabilities and convective flows in the solar interior. Mon. Not. Roy. Astron. Soc. 2009;400:337-345.

[20] Chandrasekhar S. An Introduction to the Study of Stellar Structure. 1st ed. Illinois: University of Chicago Press, 1939.

[21] Matthews PC, Proctor MRE, Weiss NO. Compressible magnetoconvection in three dimensions: planforms and nonlinear behaviour. J. Fluid Mech. 1995;305:281-305.

[22] Brummell N, Toomre J and Cattaneo F. Turbulent dynamics in the solar convection zone. 1995;269:1370-1379.

[23] Christensen-Dalsgaard J and Thompson M. Observational results and issues concerning the tachocline. In: Hughes DW, Rosner R, Weiss NO, editors. The Solar Tachocline. 1st ed. Cambridge: Cambridge University Press; 2007.

[24] Hurlburt NE, Toomre J and Massaguer JM, Two-dimensional compressible convection extending over multiple scale heights. Astrophys. J. 1984;282:557-573.

[25] Steenbeck M, Krause F and Rädler K-H. Berechnung der mittleren Lorentz–Feldstärke $u \times B$ für ein elektrisch leitendes Medium in turbulenter, durch Coriolis–Kräfte beeinflußter Bewegung. Z. Naturforschg. 1966;21a:369-376.

[26] Moffatt HK. Transport effects associated with turbulence with particular attention to the influence of helicity. Rep. Prog. Phys. 1983;46:621-664.

[27] Currie LK. The effect of magnetic field on mean flow generation by rotating two-dimensional convection. Astrophys. J. 2016;832:1-13.

[28] Busse FH. Transition to turbulence in Rayleigh-Bénard convection. In: Swinney HL, Gollub J, editors. Hydrodynamic Instabilities and the Transition to Turbulence. 2nd ed. Berlin: Springer Science & Business Media; 1985.

[29] Koschmieder EL. Bénard Cells and Taylor Vortices. 1st ed. Cambridge: Cambridge University Press; 1993.

[30] Spiegel EA. Turbulence in stellar convection zones. Comm. Astrophys. and Space Phys. 1971;3:53-58.

[31] Cline KS, Brummell NH and Cattaneo F. On the formation of magnetic structures by the combined action of velocity shear and magnetic buoyancy. Astron. Astrophys. 2003;588:630-644.

[32] Vasil GM and Brummell NH. Magnetic buoyancy instabilities of a shear-generated magnetic layer. Astrophys. J. 2008;686:709-730.

[33] Cattaneo F and Vainshtein SI. Suppression of turbulent transport by a weak magnetic field. Astrophys. J. 1991;376:L21-L24.

[34] Bushby PJ and Archontis V. Modelling magnetic flux emergence in the solar convection zone. Astron. Astrophys. 2012;545:A107.

[35] Van der Poel EP, Stevens RJAM. and Lohse D. Comparison between two- and three-dimensional Rayleigh–Bénard convection. J. Fluid Mech. 2013;736:177-194.

Peer-review history:
The peer review history for this paper can be accessed here:
https://www.sdiarticle5.com/review-history/97349